Phase Measuring Deflectometry: a new approach to measure specular free-form surfaces

Markus C. Knauer, Jürgen Kaminski and Gerd Häusler

Institute of Optics, Information and Photonics, University of Erlangen-Nuremberg,
Staudtstr. 7/B2, 91058 Erlangen, Germany

ABSTRACT

We present a new method to measure specular free-form surfaces within seconds. We call the measuring principle 'Phase Measuring Deflectometry' (PMD). With a stereo based enhancement of PMD we are able to measure both the height and the slope of the surface. The basic principle is to project sinusoidal fringe patterns onto a screen located remotely from the surface under test and to observe the fringe patterns reflected via the surface. Any slope variations of the surface lead to distortions of the patterns. Using well-known phase-shift algorithms, we can precisely measure these distortions and thus calculate the surface normal in each pixel. We will deduce the method's diffraction-theoretical limits and explain how to reach them. A major challenge is the necessary calibration. We solved this task by combining various photogrammetric methods. We reach a repeatability of the local slope down to a few arc seconds and an absolute accuracy of a few arc minutes. One important field of application is the measurement of the local curvature of progressive eyeglass lenses. We will present experimental results and compare these results with the theoretical limits.

Keywords: Optical metrology, surface normal, deflectometry, specular surfaces, calibration, stereo

1. INTRODUCTION

There is a variety of methods to measure the shape of diffusely reflecting free-form surfaces, for example fringe projection, stereo or active stereo sensing.[1] It is much more difficult, however, to measure the shape of specular free-form surfaces, since the surfaces themselves are 'not visible' – we only see their effect via the reflection of incoming light.

The measurement of optical surfaces can be done by interferometric means. However, this commonly requires complicated and expensive compensation optics.[2,3] Another option is to guide a curvature sensor along the surface.[4] Apart from interferometric methods, which measure path differences, one can also measure the deflection of reflected or transmitted light beams. One important deflectometric method is the Shack-Hartmann principle.[5] However, this method is limited concerning the dynamic range[6] and the number of measured points.

Other well-known methods for measuring aspheric surfaces are Moiré deflectometry or the 'Reflection Grating Method' introduced by Ritter et al.[7] This method is under investigation by several research groups.[8–10]

The Phase Measuring Deflectometry (PMD), which we have developed during the last years,[11–13] improves the deflectometric approaches: We measure the surface quite fast with an accuracy reaching the physical limit. We achieve this accuracy by theoretically optimized projection and observation of sinusoidal fringes. We developed a precise calibration method by combining deflectometry with photogrammetry. Deflectometric methods are ambiguous concerning the calculation of the surface normal. As the primary measure is the slope, any information about the object height is lost. Therefore most of the listed methods can only be used for qualitative inspection and not for absolute slope and height measurement. Our approach, that we consider to be new, is based on stereo and solves this ambiguity.

Further author information:
M.C.K.: E-mail: mknauer@optik.uni-erlangen.de, Telephone: +49 (0)9131 852 8385
J.K.: E-mail: jkaminski@optik.uni-erlangen.de, Telephone: +49 (0)9131 852 8385
G.H.: E-mail: haeusler@physik.uni-erlangen.de, Telephone: +49 (0)9131 852 8382
Homepage: http://www.optik.uni-erlangen.de/osmin

PMD is suitable for the measurement of various specular surfaces. This includes applications with high demands on accuracy such as the measurement of wafers or high precision optics. But the method can also be adapted for high speed inspection of bigger objects, such as painted car bodies or reflectors.

An important field of application is the measurement of progressive eyeglass lenses. In particular the surface curvature is interesting. To get the curvature from shape data, one has to calculate the second derivative. If we have already slope data, only the first derivative has to be calculated. As every derivation increases the noise, the deflectometric methods have an unbeatable advantage compared to methods that capture the shape data.

2. SENSOR PRINCIPLE

Specular objects reflect incident light in one direction only. Therefore we have to provide incoming light from many directions with a large diffusing screen so that some light will fall into the pupil of our observing camera. Figure 1 displays the setup of a sensor based on PMD.

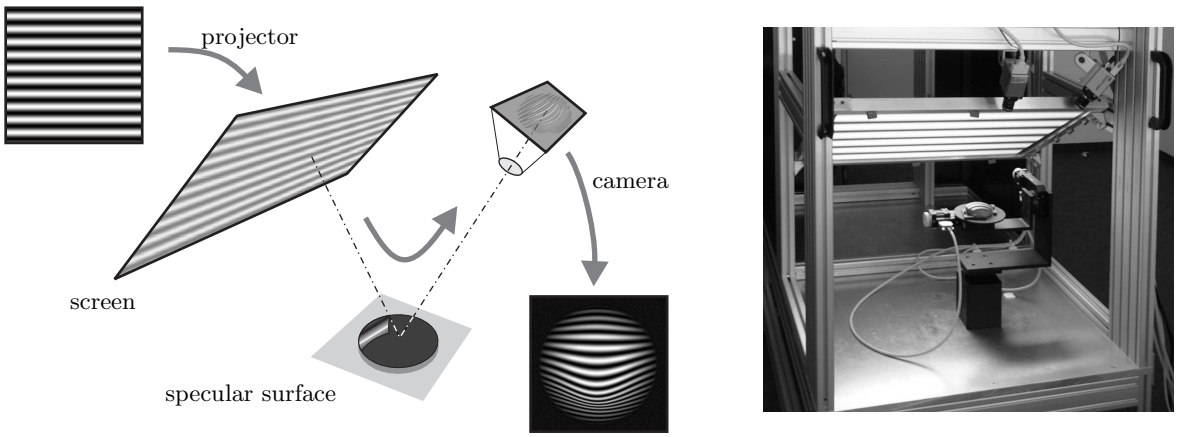

Figure 1. Left: The schematic setup of a sensor based on PMD. A projector generates fringes on a rear projection screen. A camera observes the pattern, using the specular surface as a 'mirror'. Depending on the shape of the object, the resulting fringe image is distorted. Right: Commercialized setup with positioning device. The sensor was built by our project partner 3D-Shape GmbH in Erlangen.

Compared to the 'Reflection Grating Method'[7] our new approach with PMD is the projection of sinusoidal fringe patterns: All deflectometric methods are limited by the intrinsic depth of field problem, since we cannot focus onto the object and the fringes at the same time. As the sinusoidal fringes do not change their phase when they are defocused, we can safely focus at the object. Nevertheless, the contrast of the fringes will decrease. This yields a fundamental uncertainty relation, which will be discussed in Sect. 2.1.

Figure 2 depicts one ray of light, which is reflected from the screen via the surface into the camera. In each camera pixel the phase φ of the imaged fringe pattern can be measured. Depending on the local slope of the surface and the distance d between screen and object, the phase varies according to the following equation:

$$\varphi = d \cdot \tan 2\alpha \tag{1}$$

For the evaluation of the sinusoidal pattern we can apply well-known phase-shifting-techniques. We project N fringe patterns, each shifted by $2\pi/N$. Then the phase can be calculated from the N intensities in every pixel separately.[14] Note that we have to project horizontal and vertical fringes to detect slope deviations in both azimuths (Fig. 11).

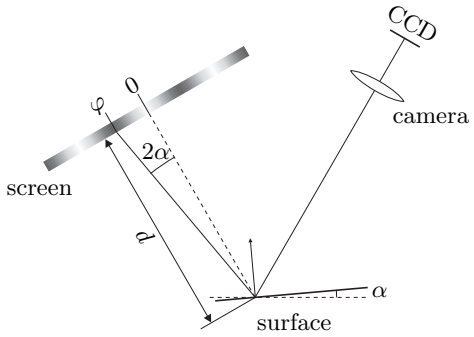

Figure 2. A ray of light that is reflected from the surface into the camera. The phase φ is a measure for the local object slope α.

2.1. Physical Limits

All measurements have to fulfill at least the Heisenberg uncertainty relation. In this case we want to measure the direction (impulse $\mathbf{p}$) and the origin (position $\mathbf{x}$) of the reflected light. These are conjugated variables. Thus we expect an uncertainty relation between the uncertainty of the measured slope $\delta\alpha$ and the measured position on the surface δx. We do not have to deduce the relation beginning at Heisenberg. Instead we can use the optical diffraction limitations. Figure 3 shows the image formation at one pixel of the camera. As stated above we focus at the object. Thus the pixel corresponds to a circle of confusion on the screen.

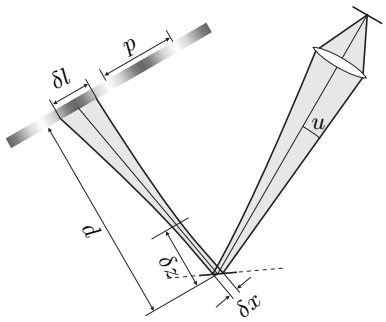

Figure 3. The camera is focused at the surface. As the depth of focus δz is shorter than the distance between object and screen, the contrast decreases. The period p must be longer than the diameter of the circle of confusion δl.

The diffraction limitation gives us the lateral resolution δx on the object according to

$$\delta x = \frac{\lambda}{\sin u}. \tag{2}$$

λ is the mean wavelength and u is the aperture of the camera. If the distance from the screen to the object is much greater than δz (which is the case in most setups) the size δl of the blurred spot on the screen can be approximated with

$$\delta l \approx 2d \sin u = 2d\frac{\lambda}{\delta x}\ , \tag{3}$$

using Eq. (2). According to Eq. (1), the angular uncertainty $\delta\alpha$ can be expressed as an uncertainty of the measured phase $\delta\varphi$:

$$\delta\varphi = 2d \cdot \tan\delta\alpha. \tag{4}$$

The uncertainty of the phase depends on several parameters. It decreases with higher contrast C and a shorter period p of the fringes. Lampalzer[14] showed that

$$\delta\varphi = \frac{p}{Q\,C}, \tag{5}$$

using a 4-shift algorithm. Q is a constant describing the phase uncertainty caused by the camera quantization error and photon noise: $Q = \Delta I/I$. What is the optimal period p? The contrast of the pattern is determined by the convolution of the blurred spot and the sinusoidal intensity distribution. In one dimension the convolution of a sinus with an rect leads to

$$C = \frac{\sin(\pi\,\delta l/p)}{\pi\,\delta l/p} \tag{6}$$

and with Eq. (5) to

$$\delta\varphi = \frac{\pi\,\delta l}{Q\,\sin(\pi\,\delta l/p)}. \tag{7}$$

Concerning the period p, the phase uncertainty gets minimal when the sinus is 1, i. e. $p = 2\delta l$. With Eq. (3) we get

$$\delta\varphi = \frac{2\pi\,\lambda\,d}{Q\,\delta x}. \tag{8}$$

Now we can merge Eqs. (4) and (8) to

$$\delta\varphi = 2d\,\tan\delta\alpha = \frac{2\pi\,\lambda d}{Q\,\delta x} \tag{9}$$

and finally achieve the expected uncertainty relation that couples the uncertainty of the slope measurement with the laterally resolvable distance:

$$\tan\delta\alpha \cdot \delta x = \frac{\pi\,\lambda}{Q}. \tag{10}$$

The relation tells us that an angular measurement at a surface element will be less accurate if the size of that surface element becomes smaller. With our laboratory setup we have a lateral resolution of $\delta x \approx 120\,\mu\text{m}$ and use a white light source with $\bar{\lambda} \approx 0.5\,\mu\text{m}$. With $Q \approx 250$ for the used 10 bit camera the theoretical $\delta\alpha$ calculates to 11 arcsec. To verify this value we measured the angular repeatability. The resulting error is approx. 12 arcsec. The experimental results show that the sensor is optimized close to the theoretical limits.

3. CALIBRATION

To calculate the local surface slope from the measured phase it is necessary to calibrate the sensor in five degrees of freedom: the position in three dimensional space and the local slope in two azimuths. The straightforward calibration procedure to measure various slopes for all possible points in the measuring volume would be very time consuming and difficult. Therefore we calibrate the system by modeling the whole sensor in the computer. The calibration is split into three separate steps: calibration of the projection (1), calibration of the camera (2) and geometric calibration of the entire system (3) (see Fig. 4). The three steps are independent and thus can be improved separately.

3.1. Projector Calibration

As mentioned before, we project horizontal and vertical fringes onto the screen. We can determine the phase φ_1 for the vertical and φ_2 for the horizontal fringes. Thus each point $\mathbf{q}$ on the screen is determined by a unique pair of phases. We define a screen coordinate system $\mathbf{X}_s$ with the $x_s y_s$ plane parallel to the screen (Fig. 4). Now we are looking for a two dimensional function

$$\mathbf{f} : \begin{pmatrix} \varphi_1 \\ \varphi_2 \end{pmatrix} \longmapsto \begin{pmatrix} x_s \\ y_s \end{pmatrix}, \tag{11}$$

which provides the correct metric position of the measured point. To find such a function we are using an aluminum plate with n precise holes at known positions. This plate is fixed tightly to the screen and the phase is measured in the middle of the holes. For each hole we get the phases φ_1^i and φ_2^i and the position $\mathbf{x}_s^i$. The function $\mathbf{f}$ is approximated by two polynomials of degree k using a Gaussian least-squares fit.[15]

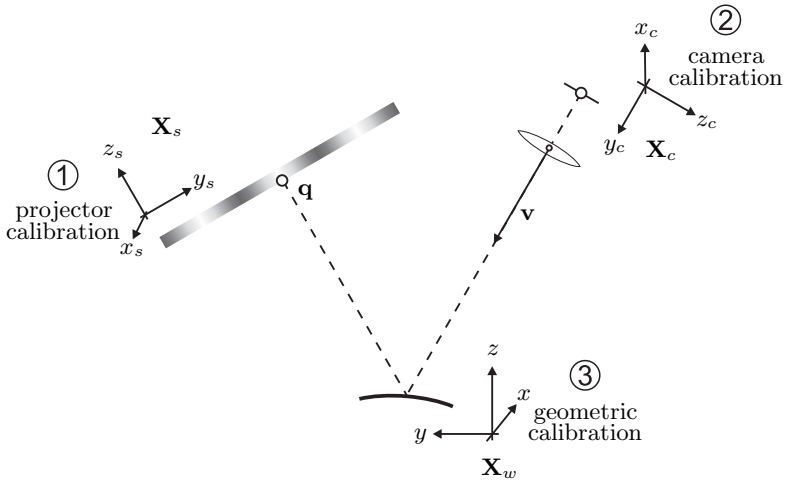

Figure 4. The calibration of the PMD sensor is divided in three steps. The geometric calibration brings together the camera and the screen coordinate system in one common coordinate system.

3.2. Camera Calibration

There are well known photogrammetric methods for the calibration of cameras. The self-calibrating method used here is based on an extended pinhole camera model by Fraser et al.[16] Again, we introduce a new coordinate system $\mathbf{X}_c$ aligned to the camera (Fig. 4). The origin $\mathbf{o}$ of the coordinate system is located in the projective center of the camera (Fig. 5).

An ideal pinhole camera would image all points placed on a straight line $\mathbf{r} = \mathbf{o} + t \cdot \mathbf{v}$ at the point $\mathbf{j}$. A real camera lens is not perfect and will image the points not at $\mathbf{j}$ but at a pixel $\mathbf{p}$. Now we are looking for a correction function

$$\mathbf{g} : \begin{pmatrix} p_x \\ p_y \end{pmatrix} \longmapsto \begin{pmatrix} j_x \\ j_y \end{pmatrix} \tag{12}$$

to calculate the ideal point $\mathbf{j}$ and thus the corresponding vector $\mathbf{v}$ for every pixel $\mathbf{p}$. See Ref. 16 for the description of the complete correction function and the distortion parameters (ten parameters modeling decentering, radial and non-orthogonality distortion). The camera parameters can be estimated by bundle adjustment methods specified in Ref. 17 using the program 'Australis'.[18] After camera calibration, for each pixel, the ray of vision $\mathbf{v}$ is defined in the camera coordinate system.

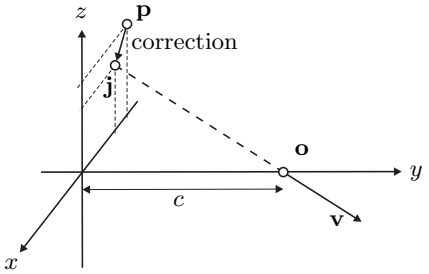

Figure 5. The extended pinhole camera model. An ideal pinhole camera would image all points in line with $\mathbf{v}$ at the point $\mathbf{j}$.

3.3. Geometric Calibration

The camera and the screen are now calibrated in different coordinate systems. Thus the third step is to transfer the coordinate systems into a common 'world' coordinate system $\mathbf{X}_w$. For this purpose we first have to find the transformation matrix $\mathbf{M}_{wc}$ from camera to world coordinates ($\mathbf{x}_w = \mathbf{M}_{wc}\,\mathbf{x}_c$). We define the world coordinate system with a set of precise marks on the surface of a flat mirror, knowing the position (in world coordinates) of each mark $\mathbf{s}_w^i$. We can find the corresponding pixel $\mathbf{p}_c^i$ in the acquired image and calculate the vector $\mathbf{v}_c^i$, in camera coordinates (Fig. 6 left). With this data we can perform a camera resection, i. e. find a Matrix $\mathbf{M}_{cw}$ that transforms the points $\mathbf{s}_w^i$ to $\mathbf{s}_c^i$ located on the rays $\mathbf{v}_c^i$. Of course the points are not exactly located on the rays but at a distance d_i. The resection calculates the matrix in such a way that the distances get minimal. Let $\|\mathbf{v}\| = 1$, then the sum to be minimized can be calculated according to

$$\sum_{i=1}^{n} \left\|d^i\right\|^2 = \sum_{i=1}^{n} \left\|\mathbf{v}_c^i \times \mathbf{s}_c^i\right\|^2 . \tag{13}$$

This yields the matrix $\mathbf{M}_{cw} = \mathbf{M}_{wc}^{-1}$. Thus the vector $\mathbf{v}_w$ is known in world coordinates. The resection can either be performed with Australis or by various numerical methods, e. g. Newton's Method.[15]

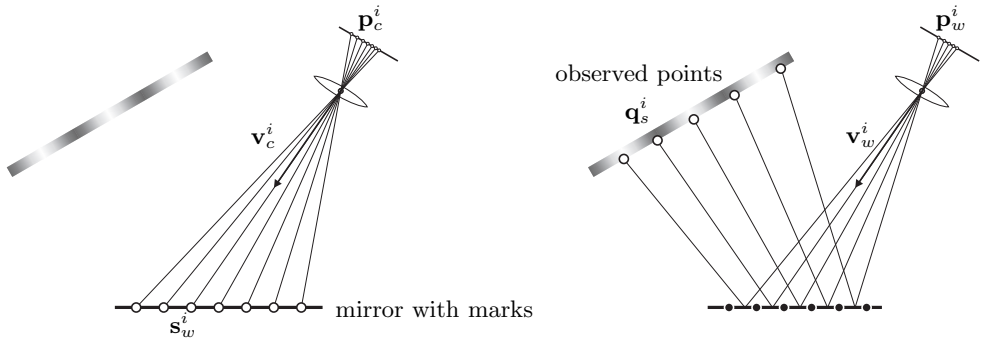

Figure 6. The geometric calibration is performed in two steps. First the position of the camera is estimated by camera resection (left). Then the position of the screen can be calculated with beams that are reflected between the marks (right).

After camera resection, the screen resection can be performed as sketched on the right of Fig. 6. As the projector is calibrated, we know the position $\mathbf{q}_s^i$ on the screen for any vector $\mathbf{v}^i$, which is reflected between the marks on the screen. Using the same resection method again we get $\mathbf{M}_{sc}$. This is the transformation from the camera coordinate system to the screen coordinate system. The desired matrix $\mathbf{M}_{ws}$ finally can be calculated according to

$$\mathbf{M}_{ws}^{*} = \mathbf{M}_{wc} \cdot \mathbf{M}_{sc}^{-1}. \tag{14}$$

As the camera observes the screen via the mirror, the resulting transformation matrix does not correspond to the position of the screen but to the position of a mirrored virtual screen. We can easily calculate the correct matrix $\mathbf{M}_{ws}$ by changing the signs of the z-components in $\mathbf{M}_{ws}^{*}$.

4. ABSOLUTE MEASUREMENT

After calibration, for each pixel $\mathbf{p}$ its ray of vision $\mathbf{v}$ and the observed point $\mathbf{q}$ are known in global coordinates. However, this information is not sufficient to calculate the surface normal. The situation is depicted in Fig. 7. The point of reflection on the surface $\mathbf{s}$ can be located anywhere on the ray of vision. The calculated normal varies depending on the assumed position. To get the real position and normal, some additional information is necessary: either the direction $\mathbf{w}$ of the incident light or the height z of the surface. Then the normal can be calculated according to

$$\mathbf{n} = -\frac{\mathbf{w} + \mathbf{v}}{\|\mathbf{w} + \mathbf{v}\|} \tag{15}$$

with $\mathbf{w} = \mathbf{s} - \mathbf{q}$ when the surface point $\mathbf{s}$ is known.

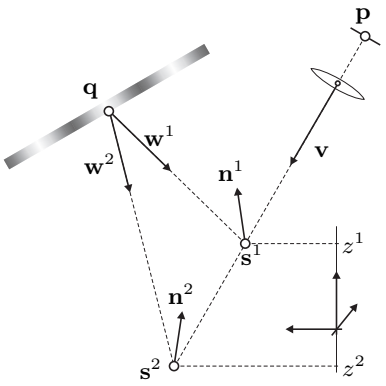

Figure 7. Where is the surface of the object located: at $\mathbf{s}^1$ or at $\mathbf{s}^2$ or in between? Although the vector $\mathbf{v}$ and the point $\mathbf{q}$ are known for each pixel, it is not possible to calculate the normal $\mathbf{n}$ without additional information.

It can be shown that the calculated normal only slightly varies with the height z. For some applications it would be enough to know the approximate height distribution of the object, e. g. from CAD data. On continuously differentiable surfaces one known surface point is enough to solve the ambiguity. Starting from this point with the correct normal, the height and normals of all other surface points can be calculated by numerical integration.[19] Nevertheless it is not easy to get even one single point on a specular surface.

Seßner proposed two methods to get the incident light vector $\mathbf{w}$.[20] One method is a telecentric setup of the sensor.[21] A lens is used to image the screen at infinity. Thus every point $\mathbf{q}$ defines only one direction $\mathbf{w}$. The limiting factor of this method is the size of the required lens and thus the dynamic range of the sensor. The other method makes use of two measurements for different screen positions and thus gets an additional point in space. This method was developed independently by Petz et al.[9] However, shifting the screen mechanically is a laborious task and takes extra time during the measurement.

4.1. Stereo Deflectometry

We introduce another solution, that we consider to be new, based on the application of a second camera. The setup is depicted in Fig. 8. Both cameras are calibrated, thus we know the positions $\mathbf{c}_i$ and the directions $\mathbf{v}_i$ for the pixels $\mathbf{p}_i$, imaging the point $\mathbf{s}$ on the surface.

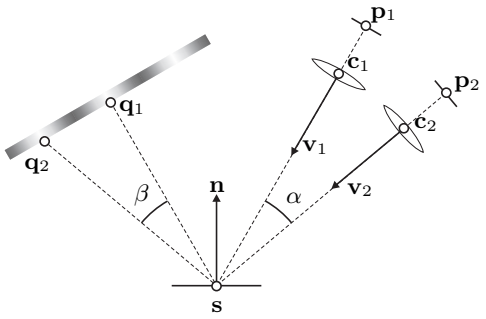

Figure 8. The setup of stereo deflectometry. A second camera is placed in the system. Though focused on the same point $\mathbf{s}$ on the object, it images another point $\mathbf{q}_2$ of the screen.

How can we solve the ambiguity explained in the last section? In active stereo (for diffusely reflecting objects) a pattern is projected directly onto the surface. The height of a point can be triangulated by searching points with the same phase in both cameras.[22] On specular surfaces we have to look for another correspondence, as

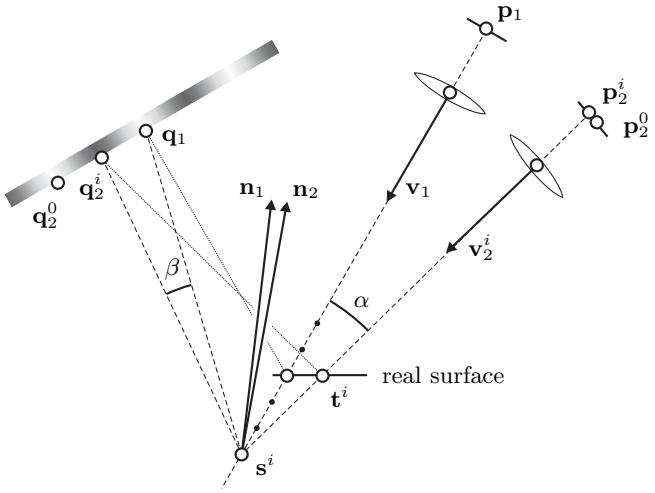

Figure 9. We find the surface points by testing several assumptions $\mathbf{s}^i$. For a wrong assumption the normals calculated from the measured points $\mathbf{q}_1$ and $\mathbf{q}_2^i$ differ for the two cameras.

the observed point $\mathbf{q}$ is not the same for the two cameras (Fig. 8). A parameter that should of course be identical for both cameras is the normal $\mathbf{n}$ on the point $\mathbf{s}$.

Our strategy is to test several assumptions for the point $\mathbf{s}$, which all are located on the ray $\mathbf{v}_1$ of the first camera. Figure 9 illustrates the situation for a wrong point $\mathbf{s}^i$ and a flat mirror. Compared to Fig. 8 with the correct point $\mathbf{s}$, the following has changed for the second camera:
The point $\mathbf{s}^i$ would be imaged at $\mathbf{p}_2^i$ instead of $\mathbf{p}_2^0$. We can find this point using the camera calibration parameters. This point $\mathbf{p}_2^i$ on the camera chip images the point $\mathbf{t}^i$ on the mirror and thus $\mathbf{q}_2^i$ instead of $\mathbf{q}_2^0$ on the screen. The wrong assumption shifts the pixel and the point on the screen. For the first camera nothing changes because the wrong point is located on the same ray as the correct point.

The normals are calculated from $\mathbf{v}_1$, $\mathbf{s}^i$ and $\mathbf{q}_1$ for the first and from $\mathbf{v}_2^i$, $\mathbf{s}^i$ and $\mathbf{q}_2^i$ for the second camera. The calculated normals $\mathbf{n}_1$ and $\mathbf{n}_2$ slightly differ for the two cameras (compare the angles α and β in Fig. 9 and in Fig. 8). So we can search for a point $\mathbf{s}^i$ that yields equal normals for both cameras.

Does this stereo method work on all surfaces? If we have a convex surface, the point $\mathbf{t}^i$ is located higher and the point $\mathbf{q}_2^i$ is located more to the left. Then the angle β is bigger and the difference between the normals is smaller or even could be zero. We have not yet dealt analytically with this problem, but it seems very unlikely that a surface leads to a difference of zero for all assumptions – especially in three dimensions. We simulated several spheric surfaces, using the sensor parameters of our laboratory setup described in Sect. 5. Figure 10 displays the angle γ between the two calculated normals depending on the height of the assumption.

The angle between the normals should get zero for the correct height z. To find the surface point $\mathbf{s}$, we can use the points next to the assumption with the lowest γ and fit a straight line. The zero of this line then estimates the height of $\mathbf{s}$. None of the simulated spheres yields an angle γ equal to zero for all assumptions. Nevertheless the gradient $\frac{d\gamma}{dx}$ is lower and thus the error of the estimated height is larger for a curvature of approx. -2.5 $^1/_{\mathrm{m}}$. On the left of Fig. 13 the height distribution of a measured sphere is depicted.

In practice we do not test assumptions that are all located on the same ray of the first camera, but test assumptions located on equidistant raster points in the measuring volume. This yields better images without perspective distortions.

5. RESULTS

At present, with stereo deflectometry we can measure the height of specular surfaces with an absolute uncertainty of about 200 µm and noise of approx. 40 µm. We will try to decrease the absolute error by some improvements of

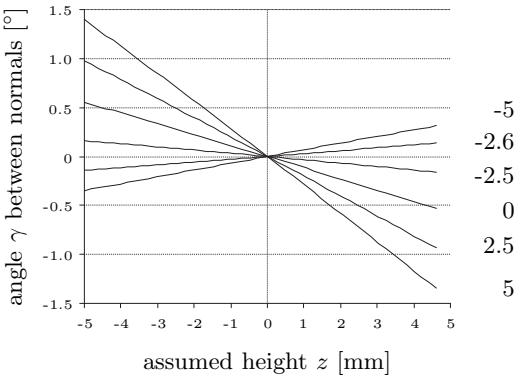

Figure 10. Simulation of the stereo method for spheric surfaces with various curvatures (denoted in $^1/_m$). The correct height is at the z-value for which the angle is zero.

the calibration. Furthermore, we will investigate the theoretical limits of the method concerning the accuracy and the ambiguity on special surfaces. In this context, the analytic investigations of Savarese et al. are promising.[23] Compared to other methods for solving the height ambiguity, we do not have to shift the screen and do not need a telecentric lens. The method is fast and scalable from small objects like lenses to large objects like painted car bodies.

A main field of application is the measurement of progressive eyeglass lenses. The screen in our setup has a size of approx. $600\times500\,\mathrm{mm}^2$, the distance from the object to the screen is approx. 250 mm and our measuring field has a diameter of approx. 100 mm. We use two digital cameras with a resolution of 1000×1000 pixels, which yields a lateral resolution of approx. 100 µm. Figure 11 shows the fringes on a progressive eyeglass lens. The local phase offset of the fringes depends on the local slope. A higher curvature of the surface means a faster change of the slope and thus a higher spacial frequency of the fringes. At present, we are taking 20 images for a complete measurement. The resulting acquisition time for one measurement is about 10 seconds.

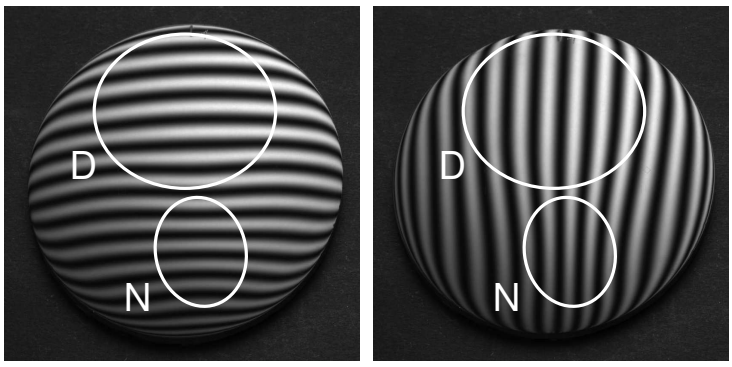

Figure 11. Distorted fringes on a progressive eyeglass lens. The distance portion and the near portion are marked with D and N.

The main interest is the knowledge of the surface power $S = (n-1)\cdot 1/R$ at every point of the surface. n is the refractive index of the material (usually set to 1.525). The methods used for calculating the curvature $1/R$ from discrete slope data are explained in Ref. 24. On free-form surfaces however, one has to consider the two principal curvatures κ_1 and κ_2 and their direction. Of special interest for the optical properties of eyeglass lenses are the local mean surface power $\overline{S} = (n-1)\cdot(\kappa_1+\kappa_2)/2$ and the local astigmatism of the surface $\Delta S = (n-1)\cdot(\kappa_1-\kappa_2)$.

The measurement of the lens depicted in Fig. 11 leads to the maps of Fig. 12. The local curvature was

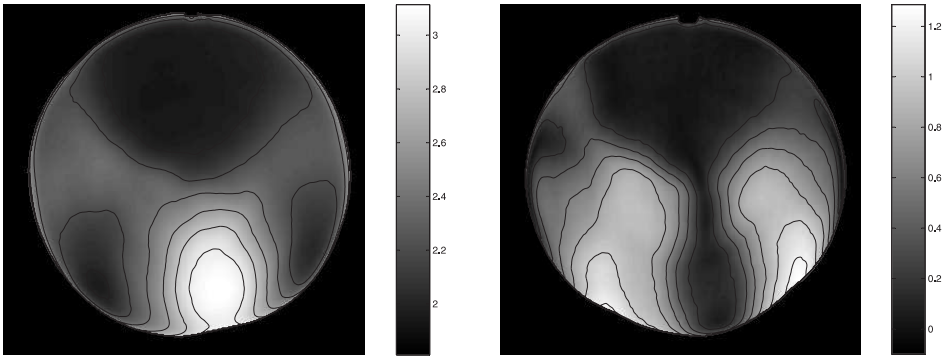

Figure 12. Curvature maps of a progressive eyeglass lens. Left: The local mean surface power $\overline{S}$ is approx. 2 dpt in the distance portion and approx. 3 dpt in the near portion. Right: The local surface astigmatism ΔS is very low in the large distance portion on the top and in the smaller near portion on the bottom.

calculated using areas of only $3\times3\,\mathrm{mm}^2$. The resulting peak-to-peak waviness is lower than 0.01 dpt. This fulfills the requirements from the manufacturers and is close to the physical limit deduced in Sect. 2.1. A curvature variation of 0.01 dpt on a distance of 3 mm is equivalent to a dent with a depth of only 20 nm.

To test the absolute calibration of the sensor, we measured a precise spherical lens at two positions shifted by 5 mm. Figure 13 displays the cross sections through the resulting height and mean surface power map. The nominal surface power of the sphere is 6.562 dpt. In the middle of the measuring field the absolute error is below 0.01 dpt. The standard deviation of the calculated surface power is 0.003 dpt.

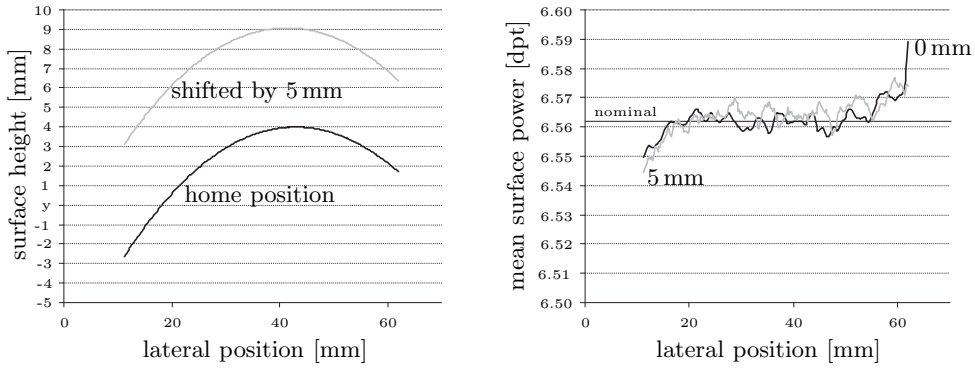

Figure 13. Measurement of a precise spherical lens. Left: The lens was measured in two positions. Right: The measured curvature is very close to the nominal value for both positions, thus confirming that our calibration is reliable.

ACKNOWLEDGMENTS

This project was funded by the 'Bayerische Forschungsstiftung'(AZ 450/01). We thank our project partners for their contributions.

REFERENCES

1. B. Jähne, H. Haußecker, and P. Geißler, eds., *Handbook of Computer Vision and Applications.*, vol. 1. Sensors and Imaging, Acdemic Press, Boston, 1999.
2. M. Beyerlein, N. Lindlein, and J. Schwider, "Dual-wave-front computer-generated holograms for quasi-absolute testing of aspherics," *Applied Optics* **41**, pp. 2440–7, May 2002.

3. H. Tiziani, S. Reichelt, C. Pruss, M. Rocktaschel, and U. Hofbauer, "Testing of aspheric surfaces," in *Lithographic and Micromachining Techniques for Optical Component Fabrication. 29-30 July 2001 San Diego, CA, USA*, *Proceedings of the SPIE* **4440**, pp. 109–19, July 2001.
4. I. Weingärtner, M. Schulz, P. Thomsen-Schmidt, and C. Elster, "Measurement of steep aspheres: a step forward to nanometer accuracy," in *Optical Metrology Roadmap for the Semiconductor, Optical, and Data Storage Industries II, San Diego, CA, USA*, *Proceedings of the SPIE* **4449**, pp. 195–204, August 2001.
5. J. Pfund, N. Lindlein, J. Schwider, R. Burow, T. Blumel, and K.-E. Elssner, "Absolute sphericity measurement: a comparative study of the use of interferometry and a shack-hartmann sensor," *Optics Letters* **23**, pp. 742–4, May 1998.
6. M. Rocktäschel and H. Tiziani, "Limitations of the shack-hartmann sensor for testing optical aspherics," *Optics and Laser Technology* **34**, pp. 631–7, November 2002.
7. R. Ritter and R. Hahn, "Contribution to analysis of the reflection grating method," *Optics and Lasers in Engineering* **4**(1), pp. 13–24, 1983.
8. D. Pérard and J. Beyerer, "Three-dimensional measurement of specular free-form surfaces with a structured-lighting reflection technique," in *Three-Dimensional Imaging and Laser-based Systems for Metrology and Inspection III, Pittsburgh, PA, USA*, *Proceedings of the SPIE* **3204**, pp. 74–80, October 1997.
9. M. Petz and R. Tutsch, "Measurement of optically effective surfaces by imaging of gratings," in *Optical Measurement Systems for Industrial Inspection II, Munich, Germany*, *Proceedings of the SPIE* **5144**, pp. 288–94, June 2003.
10. S. Kammel, "Deflectometry for quality control of specular surfaces," *Technisches Messen tm* **70**, pp. 193–8, April 2003.
11. G. Häusler, "Verfahren und Vorrichtung zur Ermittlung der Form oder der Abbildungseigenschaften von spiegelnden oder transparenten Objekten." Patent DE 19944354 A1, 1999.
12. C. Horneber, M. Knauer, and G. Häusler, "Phase measuring deflectometry – a new method to measure reflecting surfaces," annual report, Lehrstuhl für Optik, University of Erlangen-Nuremberg, 2000. See homepage for download.
13. G. Häusler, C. Horneber, and M. Knauer, "Physical limits of phase measuring deflectometry," annual report, Lehrstuhl für Optik, University of Erlangen-Nuremberg, 2001. See homepage for download.
14. R. Lampalzer, *Physikalische und informationstheoretische Eigenschaften und Grenzen von Systemen zur optischen Formerfassung und Inspektion nach dem Prinzip der phasenmessenden Triangulation.* PhD thesis, University of Erlangen-Nuremberg, 2003.
15. W. H. Press, S. A. Teukolsy, W. T. Vetterling, and B. P. Flannery, *Numerical Recipes in C: The Art of Scientific Computing*, Cambridge University Press, 2 ed., 1992.
16. C. S. Fraser, "Digital camera self-calibration," *ISPRS Journal of Photogrammetry & Remote Sensing* **52**, pp. 149–159, 1997.
17. C. S. Fraser, "Photogrammetric camera component calibration: A review of analytical techniques," in *Calibration and Orientation of Cameras in Computer Vision*, A. Gruen and T.-S. Huang, eds., *Springer Series in Information Sciences* **34**, ch. 4, pp. 95–121, Springer, 2001.
18. C. S. Fraser et al., "Australis 6.0." University of Melbourne, Department of Geomatics, 2002.
19. K. Schlüns and R. Klette, "Local and global integration of discrete vector fields," in *Advances in Computer Vision, 8th TFCV workshop, Dagstuhl*, Springer, 1996.
20. R. Seßner, "Phasenmessende Deflektometrie (PMD) - ein hochgenaues Verfahren zur Vermessung spiegelnder Oberflächen." Zulassungsarbeit, University of Erlangen-Nuremberg, 2000.
21. R. Seßner, "Verfahren zum optischen Messen der Form spiegelnder Oberflächen." Patent DE 10014964 C2, 2000.
22. K. Veit, *Verringerung systematischer Meßfehler bei der phasenmessenden Triangulation durch Kalibration.* PhD thesis, University of Erlangen-Nuremberg, 2003.
23. S. Savarese, Min-Chen, and P. Perona, "Second order local analysis for 3d reconstruction of specular surfaces," in *Proceedings First International Symposium on 3D Data Processing Visualization and Transmission, Padova, Italy*, G. Cortelazzo and C. Guerra, eds., pp. 356–61, IEEE, June 2002.
24. J. Kaminski, M. Knauer, and G. Häusler, "Calculating curvatures from discrete slope data," annual report, Lehrstuhl für Optik, University of Erlangen-Nuremberg, 2003. See homepage for download.